Journal of Applied Mechanics and Technical Physics, Vol. 52, No. 6, pp. 896–904, 2011

NUMERICAL STUDY OF SPATIAL SUPERSONIC FLOW OF A PERFECT GAS WITH TRANSVERSE INJECTION OF JETS

A. O. Beketaeva and A. Zh. Naimanova

UDC 532.526

Three-dimensional supersonic turbulent flow in the presence of symmetric transverse injection of round jets through slots in the walls is studied numerically. The simulation is based on Favre averaged Navier–Stokes equations solved using the Beam–Warming method. The influence of the ratio of the pressure in the jet to that in the flow (pressure ratio) on the spatial interaction of the injected jet with the oncoming flow is studied. Experimental pressure distributions on the wall near the jet approximated by curvilinear closed ellipses are reproduced numerically. The mechanism of the formation of two symmetric vortices in the mixing layer between the jet and the oncoming flow is studied. The results of the calculations are found to be in satisfactory agreement with the experimental dependence of the length of the separation zone on the pressure ratio of the jet to the flow.

Keywords: *supersonic flow, Navier–Stokes equations, pressure ratio, Mach number, numerical simulation.*

DOI: 10.1134/S0021894411060071

Introduction. Interest in the interaction of a transverse jet with supersonic flow is due primarily to the development of new designs of vertical take-off and landing aircraft, aircraft thrust vector control systems, and ramjets.

The spatial flow of a sonic jet to supersonic flow has been studied for a long time. The results of studying the interaction of a transverse jet with oncoming flow [1–3] show that, as in the case of the plane problem [4–7], a bow shock, an oblique shock, and a terminal shock occur in front of the jet and intersect at one point to form a complex λ-shaped system of shocks. In the flow diagram shown in Fig. 1, these shocks are shown by lines 1–3. The flow-off line 5 corresponds to the boundary of the shock 2, behind which there is a region of boundary-layer separation in front of the jet. A tail shock forms on the flow-off line 6. It is known that this shock forms behind an injection nozzle when the flow enveloping the injected jet impinges on the wall. The spreading line 7 is the boundary of the terminal shock 3, on which the flow from the high-pressure region spreads in all directions. Most of the flow turns down to the wall and enters the zone of oppositely directed separation flow. Upon reaching the wall, the flow spreads over it from line 7 in opposite directions. One part of the flow moves toward the main flow, and the other turns to the jet. As a consequence, two spatial vortices rotating in opposite directions arise in the flow separation zone in front of the jet, and a horseshoe-shaped vortex system of inhomogeneous structure is formed [1, 7]. The generalized gas-dynamic pattern of interaction of the injected jet with the oncoming flow is also shown in [2, 3].

An analysis of papers [8, 9] devoted to the numerical simulation of supersonic spatial flows of a monatomic gas shows that a detailed study of the dependence of the structure of the flows on the parameters of the problem have not been made. Because of the complexity of the numerical solution of such problems, many papers focus

Institute of Mathematics, Ministry of Education and Science of the Republic of Kazakhstan, Alma Ata 050010, Kazakhstan; ked@math.kz. Translated from Prikladnaya Mekhanika i Tekhnicheskaya Fizika, Vol. 52, No. 6, pp. 58–68, November–December, 2011. Original article submitted April 6, 2010; revision submitted January 11, 2011.

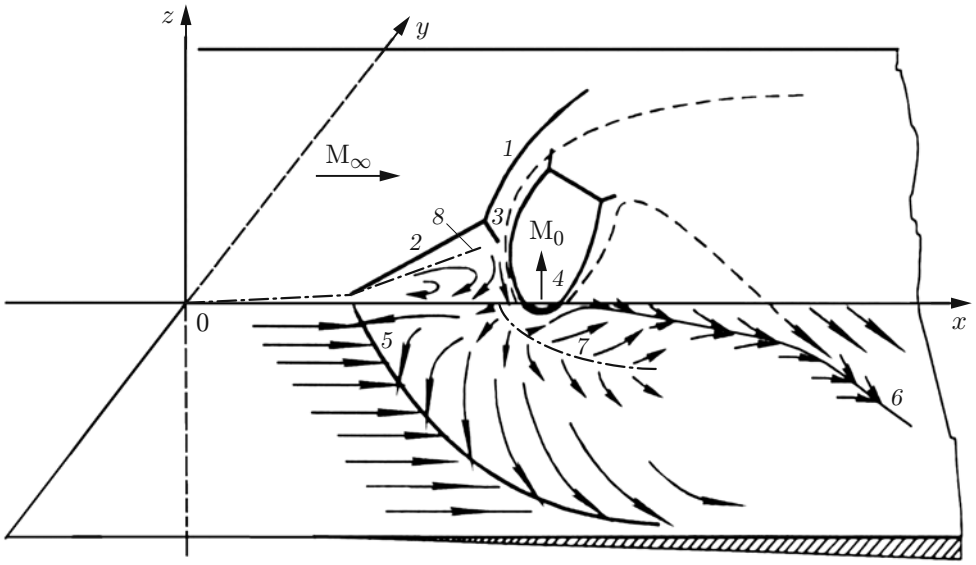

Fig. 1. Flow diagram: bow shock (1), oblique shock (2), terminal shock (3), jet issuing into the flow (4), boundary of the oblique shock (5), flow-off line (6), and flow spreading lines (7 and 8); the dashed line shows the boundary of the injected jet; the arrows shows the streamlines.

on the development of methods of solution or turbulence models (see, e.g., [8, 9]). From these studies, it follows that the shock-wave structure and dimension of the separation region significantly depend on the parameters of the problem. For example, the injection of a supersonic jet into a supersonic flow at an angle of 25° to the streamlined plate has been simulated numerically [8]. Turbulent flow is described using Reynolds stress equations. Computer simulation [8] has shown that in a jet there is a pair of vortices. The interaction of supersonic turbulent flow with a jet injected from a square hole on a wall perpendicular to the flow has been studied numerically [9] using a nonoscillating weight scheme of high-order approximation. The data reported in [9] does not imply the existence of paired vortices in the jet. This indicates a need for further investigation of the interaction of a jet with oncoming flow.

The purpose of the present work was a numerical simulation of the injection of a round sonic jet perpendicular to supersonic flow in a rectangular channel. For convenience of calculations, we consider the injection of a jet only from the bottom wall (see Fig. 1). To solve this problem, we extend the Beam–Warning method to the three-dimensional case and introduce additional diffusion terms of the fourth order. (Previously [10], it has been shown for the plane problem that this numerical method provides fairly accurate calculations of supersonic flow of a monatomic gas in the presence of perpendicular injection of jets.) The effect of the pressure ratio on the shock-wave structure of the flow is studied.

Formulation of the Problem. The initial system consists of three-dimensional Favre-averaged Navier–Stokes equations for turbulent flow of a compressible gas, written in Cartesian coordinates in conservative form:

$$\frac{\partial \boldsymbol{U}}{\partial t} + \frac{\partial (\boldsymbol{E} - \boldsymbol{E}_v)}{\partial x} + \frac{\partial (\boldsymbol{F} - \boldsymbol{F}_v)}{\partial z} + \frac{\partial (\boldsymbol{G} - \boldsymbol{G}_v)}{\partial y} = 0. \tag{1}$$

Here the vectors $\boldsymbol{U}$, $\boldsymbol{E}$, $\boldsymbol{F}$, and $\boldsymbol{G}$ are given by the expressions

$$\boldsymbol{U} = \begin{pmatrix} \rho \\ \rho u \\ \rho v \\ \rho w \\ E_t \end{pmatrix}, \quad \boldsymbol{E} = \begin{pmatrix} \rho u \\ \rho u^2 + P \\ \rho uv \\ \rho uw \\ (E_t + P)u \end{pmatrix}, \quad \boldsymbol{F} = \begin{pmatrix} \rho w \\ \rho uw \\ \rho vw \\ \rho w^2 + P \\ (E_t + P)w \end{pmatrix}, \quad \boldsymbol{G} = \begin{pmatrix} \rho v \\ \rho uv \\ \rho v^2 + P \\ \rho vw \\ (E_t + P)v \end{pmatrix},$$

the vectors $\boldsymbol{E}_v$, $\boldsymbol{F}_v$, and $\boldsymbol{G}_v$ are related to viscous stresses as

$$\boldsymbol{E}_v = (0, \tau_{xx}, \tau_{xy}, \tau_{xz}, u\tau_{xx} + v\tau_{xz} + w\tau_{xz} - q_x)^{\mathrm{t}},$$

$$\boldsymbol{F}_v = (0, \tau_{xz}, \tau_{yz}, \tau_{zz}, u\tau_{xz} + v\tau_{yz} + w\tau_{zz} - q_z)^{\mathrm{t}},$$

$$\boldsymbol{G}_v = (0, \tau_{xy}, \tau_{yy}, \tau_{yz}, u\tau_{xy} + v\tau_{yy} + w\tau_{yz} - q_y)^{\mathrm{t}},$$

the components of the stress tensor and heat flux vector are expressed as

$$\tau_{xx} = \frac{2}{3}\frac{\mu_t}{\mathrm{Re}}(2u_x - w_z - v_y), \quad \tau_{zz} = \frac{2}{3}\frac{\mu_t}{\mathrm{Re}}(2w_z - u_x - v_y), \quad \tau_{yy} = \frac{2}{3}\frac{\mu_t}{\mathrm{Re}}(2v_y - u_x - w_z),$$

$$\tau_{xz} = \tau_{zx} = \frac{\mu_t}{\mathrm{Re}}(u_z + w_x), \quad \tau_{xy} = \tau_{yx} = \frac{\mu_t}{\mathrm{Re}}(u_y + v_x), \quad \tau_{yz} = \tau_{zy} = \frac{\mu_t}{\mathrm{Re}}(w_y + v_z),$$

$$q_x = -\frac{\mu_t}{(\gamma-1)\mathrm{M}_\infty^2 \mathrm{Pr}\,\mathrm{Re}}T_x, \quad q_y = -\frac{\mu_t}{(\gamma-1)\mathrm{M}_\infty^2 \mathrm{Pr}\,\mathrm{Re}}T_y, \quad q_z = -\frac{\mu_t}{(\gamma-1)\mathrm{M}_\infty^2 \mathrm{Pr}\,\mathrm{Re}}T_z,$$

the pressure P and the temperature T are given by

$$P = (\gamma-1)\Big[E_t - \frac{1}{2}(\rho u^2 + \rho w^2 + \rho v^2)\Big], \qquad T = \frac{1}{\rho c_v}\Big[E_t - \frac{1}{2}(\rho u^2 + \rho w^2 + \rho v^2)\Big], \qquad c_v = \frac{1}{\gamma(\gamma-1)\mathrm{M}_\infty^2},$$

where t is time, u, w, and v are the components of the flow velocity in the longitudinal and transverse directions, ρ is the density, c_v is the specific heat at constant volume, γ is the adiabatic exponent, M_0 and M_∞ are the Mach numbers of the jet and flow, μ_t is the turbulent viscosity, Re is the Reynolds number, and Pr is the Prandtl number; the subscript ∞ corresponds to the flow parameters.

The basic system of equations (1) is written in dimensionless form. The governing parameters are taken to be the input parameters u_∞, ρ_∞, and T_∞, the pressure and total energy are normalized by the value of $\rho_\infty u_\infty^2$, and the characteristic length scale is the diameter of the hole. System (1) is closed by means of the Baldwin–Lomax algebraic turbulence model [11].

The boundary conditions are as follows:

— at the inlet ($x = 0$, $0 \leqslant y \leqslant H_y$, $0 \leqslant z \leqslant H_z$),

$$u = 1, \quad v = 0, \quad w = 0, \quad \rho = 1, \quad T = 1;$$

— on the bottom wall ($z = 0$, $0 < x \leqslant H_x$, $0 \leqslant y \leqslant H_y$),

$$u = 0, \quad v = 0, \quad w = 0, \quad \frac{\partial T}{\partial z} = 0, \quad \frac{\partial P}{\partial z} = 0;$$

— in the jet ($z = 0$ and $|x^2 + y^2| \leqslant R$),

$$u = 0, \quad v = 0, \quad T = 0.6, \quad w = \sqrt{T}\,\mathrm{M}_0/\mathrm{M}_\infty, \quad P = nP_\infty$$

($n = P_0/P_\infty$ is the pressure ratio, P_0 is the pressure in the jet, and P_∞ is the pressure in the flow; the subscript 0 corresponds to the parameters of the jet).

A boundary layer is specified near the wall, and the longitudinal velocity component is approximated as follows [4, 12]:

$$u = 0.1z/\delta_2 + 0.9(z/\delta_2)^2, \qquad 0 \leqslant x \leqslant H_x, \quad 0 \leqslant z \leqslant \delta_2, \quad z^+ \leqslant 70,$$

$$u = (z/\delta_1)^{1/7}, \qquad 0 \leqslant x \leqslant H_x, \quad \delta_2 \leqslant z \leqslant \delta_1, \quad z^+ \geqslant 70.$$

Here $\delta_2 = 0.2\delta_1$ is the thickness of the near-wall layer, $\delta_1 = 0.37x(\mathrm{Re}_x\, x)^{-0.2}$ is the thickness of the boundary layer, $z^+ = \delta_2(u_\tau\,\mathrm{Re}_x)$, $u_\tau = (C_f/2)^{1/2}u_\infty$, and C_f is the flow friction coefficient on the wall.

The upper boundary ($z = H_z$, $0 < x \leqslant H_x$, and $0 \leqslant y \leqslant H_y$) is subject to the symmetry condition

$$w = 0, \quad \frac{\partial u}{\partial z} = 0, \quad \frac{\partial v}{\partial z} = 0, \quad \frac{\partial T}{\partial z} = 0,$$

and the lateral boundaries ($y = 0$, $y = H_y$, $0 < x \leqslant H_x$, and $0 \leqslant z \leqslant H_z$) are subject to the condition

$$\frac{\partial u}{\partial y} = \frac{\partial v}{\partial y} = \frac{\partial w}{\partial y} = \frac{\partial \rho}{\partial y} = 0$$

(H_x, H_z, and H_y are the length, height, and width of the computational domain, respectively; R is the hole radius).

At the outlet boundary, the nonreflection condition is specified [13].

Method of Solution. For more accurate accounting of the flow in the boundary layer, near the wall (along the z coordinate), and in the vicinity of the slot, i.e., in regions of large gradients, the grid is refined in the longitudinal and transverse directions with the help of the transformations

$$\xi = \xi(x), \qquad \zeta = \zeta(y), \qquad \eta = \eta(z).$$

In this case, system (1) linearized with respect to the vector $\tilde{\boldsymbol{U}}$ can be written in the generalized coordinates as

$$\Big\{I + \Delta t\Big[\frac{\partial A_\xi^n}{\partial \xi} + \frac{\partial B_\eta^n}{\partial \eta} + \frac{\partial Q_\zeta^n}{\partial \zeta} - \frac{\partial}{\partial \xi}\frac{\mu_t \xi_x^2}{\mathrm{Re}\, J}\frac{\partial}{\partial \xi}\frac{1}{U_1^n} - \frac{\partial}{\partial \eta}\frac{\mu_t \eta_z^2}{\mathrm{Re}\, J}\frac{\partial}{\partial \eta}\frac{1}{U_1^n} - \frac{\partial}{\partial \zeta}\frac{\mu_t \zeta_y^2}{\mathrm{Re}\, J}\frac{\partial}{\partial \zeta}\frac{1}{U_1^n}\Big]\Big\}\tilde{\boldsymbol{U}}^{n+1}$$

$$= \tilde{\boldsymbol{U}}^n + \Delta t\Big[2\Big(\frac{\partial \tilde{\boldsymbol{E}}_{vm}^n}{\partial \xi} + \frac{\partial \tilde{\boldsymbol{F}}_{vm}^n}{\partial \eta} + \frac{\partial \tilde{\boldsymbol{G}}_{vm}^n}{\partial \zeta}\Big) - \Big(\frac{\partial \tilde{\boldsymbol{E}}_{vm}^{n-1}}{\partial \xi} + \frac{\partial \tilde{\boldsymbol{F}}_{vm}^{n-1}}{\partial \eta} + \frac{\partial \tilde{\boldsymbol{G}}_{vm}^{n-1}}{\partial \zeta}\Big)$$

$$+ \frac{\partial \tilde{\boldsymbol{E}}_{v22}^n}{\partial \xi} + \frac{\partial \tilde{\boldsymbol{F}}_{v22}^n}{\partial \eta} + \frac{\partial \tilde{\boldsymbol{G}}_{v22}^n}{\partial \zeta}\Big] + O(\Delta t^2), \tag{2}$$

where $\tilde{\boldsymbol{U}} = J^{-1}\boldsymbol{U}$, $J = \partial(\xi, \eta, \zeta)/\partial(x, z, y)$ is the Jacobian of the transformation, $A_\xi = \xi_x A$, $B_\eta = \eta_z B$, $Q_\zeta = \zeta_y Q$, $A = \partial \boldsymbol{E}/\partial \boldsymbol{U}$, $B = \partial \boldsymbol{F}/\partial \boldsymbol{U}$, and $Q = \partial \boldsymbol{G}/\partial \boldsymbol{U}$ are Jacobian matrices. The diffusion terms are represented as the sum of the second derivatives of the required vector $\boldsymbol{U}$ with variable viscosities and the vectors $\tilde{\boldsymbol{E}}_{v22}^n$, $\tilde{\boldsymbol{F}}_{v22}^n$, and $\tilde{\boldsymbol{G}}_{v22}^n$ containing the remaining, dissipative, terms.

The diffusion flow vectors with the mixed derivatives $\tilde{\boldsymbol{E}}_{vm}$, $\tilde{\boldsymbol{F}}_{vm}$, and $\tilde{\boldsymbol{G}}_{vm}$ are approximated using an explicit scheme with a uniform time step of second-order accuracy [14].

System (2) is solved by the Beam–Warming method. For this, system (2) is subject to factorization, which reduces the problem to three one-dimensional equations which are solved by using matrix sweep:

$$\Big\{I + \Delta t\Big[\frac{\partial A_\xi^n}{\partial \xi} - \frac{\partial}{\partial \xi}\frac{\mu_t \xi_x^2}{\mathrm{Re}\, J}\frac{\partial}{\partial \xi}\frac{1}{U_1^n}\Big]\Big\}\boldsymbol{U}^* = \mathbf{RHS}^n,$$

$$\Big\{I + \Delta t\Big[\frac{\partial B_\eta^n}{\partial \eta} - \frac{\partial}{\partial \eta}\frac{\mu_t \eta_z^2}{\mathrm{Re}\, J}\frac{\partial}{\partial \eta}\frac{1}{U_1^n}\Big]\Big\}\boldsymbol{U}^{**} = \boldsymbol{U}^*,$$

$$\Big\{I + \Delta t\Big[\frac{\partial Q_\zeta^n}{\partial \zeta} - \frac{\partial}{\partial \zeta}\frac{\mu_t \zeta_y^2}{\mathrm{Re}\, J}\frac{\partial}{\partial \zeta}\frac{1}{U_1^n}\Big]\Big\}\tilde{\boldsymbol{U}}^{n+1} = \boldsymbol{U}^{**}$$

[$\mathbf{RHS}^n$ is the right side of Eqs. (2)].

In the approximation of the derivatives with respect to the spatial coordinates, the convective and diffusion terms use central-difference operators of second-order accuracy.

Analysis of the Calculation Results. In the calculations, we used coordinate transformations of the form [15]

$$\xi = K + \frac{1}{\tau}\,\mathrm{arsh}\Big[\Big(\frac{x}{x_c} - 1\Big)\sinh(\tau K)\Big],$$

$$\eta = H\Big[\beta + 1 - (\beta - 1)\Big(\frac{\beta + 1}{\beta - 1}\Big)^{1 - z/a}\Big] \Big/ \Big[\Big(\frac{\beta + 1}{\beta - 1}\Big)^{1 - z/a} + 1\Big],$$

$$\zeta = K + \frac{1}{\tau}\,\mathrm{arsh}\Big[\Big(\frac{y}{y_c} - 1\Big)\sinh(\tau K)\Big],$$

where

$$K = \frac{1}{2\tau}\ln\Big[\Big(1 + (\mathrm{e}^\tau - 1)\,\frac{x_c}{L}\Big) \Big/ \Big(1 - (\mathrm{e}^\tau - 1)\,\frac{x_c}{L}\Big)\Big],$$

$\beta > 1$ and $\tau > 1$ are the refinement parameters, a is the height of the computational domain in the generalized coordinates, and x_c and y_c are points relative to which the refinement is carried out.

To suppress high-frequency perturbations, in the last step we performed fourth-order smoothing with a small coefficient ε at the smoothing terms. The calculation was performed on a spatially staggered $201 \times 101 \times 81$ grid with steps $\Delta x = 0.1$–0.5, $\Delta z = 0.06$–0.25, and $\Delta y = 0.1$–0.5; the time step was varied in the range $\Delta t = 0.025$–0.050.

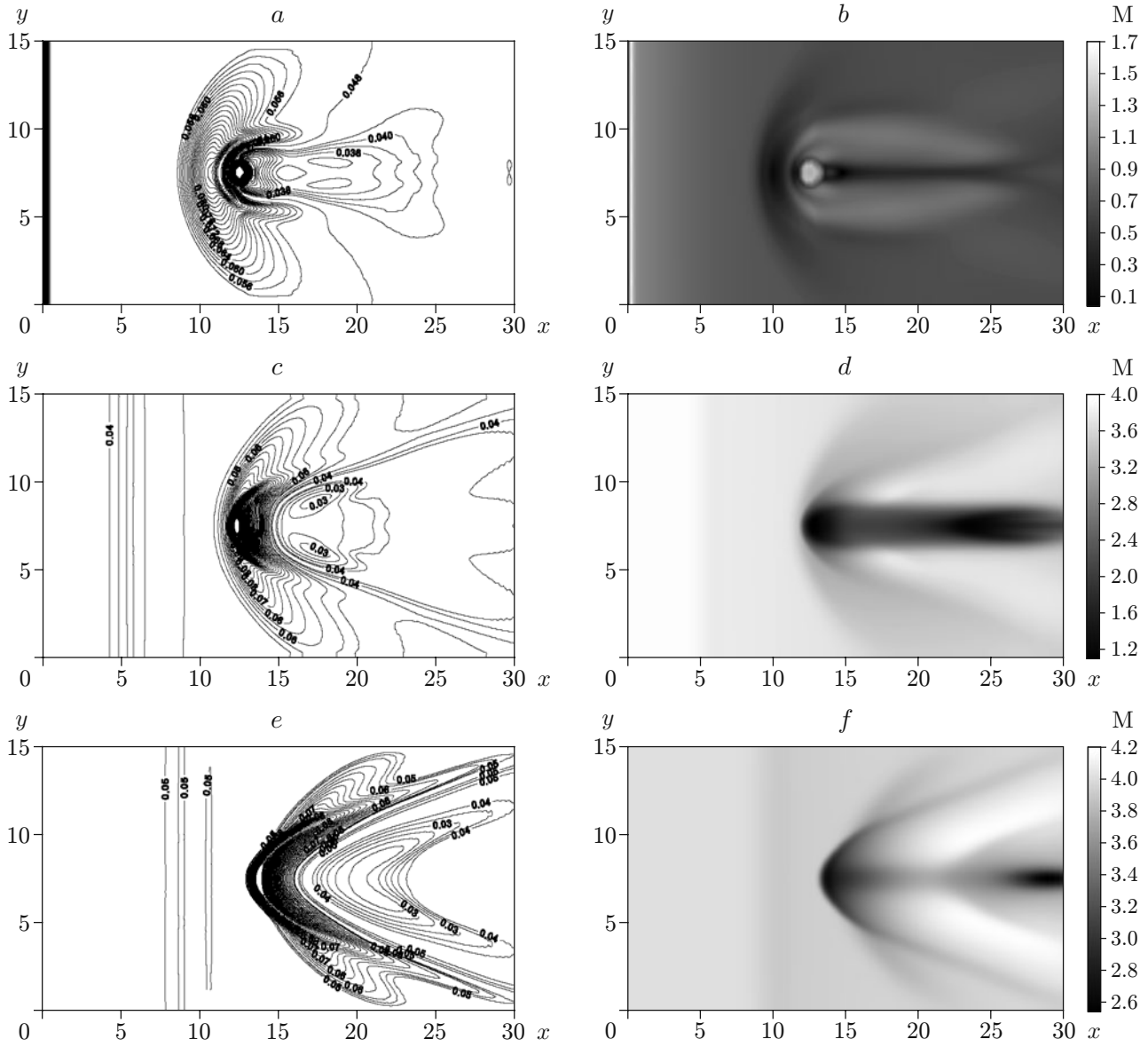

Fig. 2. Isobars (a, c, and e) and the distribution of the local Mach number (b, d, and f) in the plane x, y at different sections of z for $M_\infty = 4$, $M_0 = 1$, $n = 10$, $Pr = 0.9$, $Re = 10^4$, and $\gamma = 1.4$: (a, b) $z = 0.063$; (c, d) $z = 1.01$; (e, f) $z = 1.8$.

To validate the numerical method, we solved a test problem in a two-dimensional formulation with symmetry conditions on the boundaries. We considered transverse air flow ($M_\infty = 2.9$, $T = 108$ K, and $P = 0.0663$ MPa) over a gas jet ($M_0 = 1$, $T = 217$ K, and $P = 1.24$ MPa) issuing from a slot 0.0559 cm wide in a rectangular channel. The height of the channel was 7.62 cm, and its length was 15 cm. The calculated velocity and pressure fields at the wall reported in [10] are in satisfactory agreement with experimental data [4, 5].

Numerical calculations were performed for the following values of the characteristic parameters: $Pr = 0.9$, $M_0 = 1$, $2 \leqslant M_\infty \leqslant 4$, and $4 \leqslant n \leqslant 15$, the distance from the inlet boundary to the center of the jet was $x_0 = 12.5$ calibers, $H_x = 30$ calibers, $H_z = 10$ calibers, $H_y = 15$ calibers.

Figures 2a, 2c, and 2e show isobars (pressure in millipascals) in the plane x, y in various sections of z. In the experiments of [1–3], the pressure distribution on the wall near the jet, i.e., isobaric curves, were approximated by curvilinear closed nested ellipses, the pressure along which was constant. The numerical experiments confirm

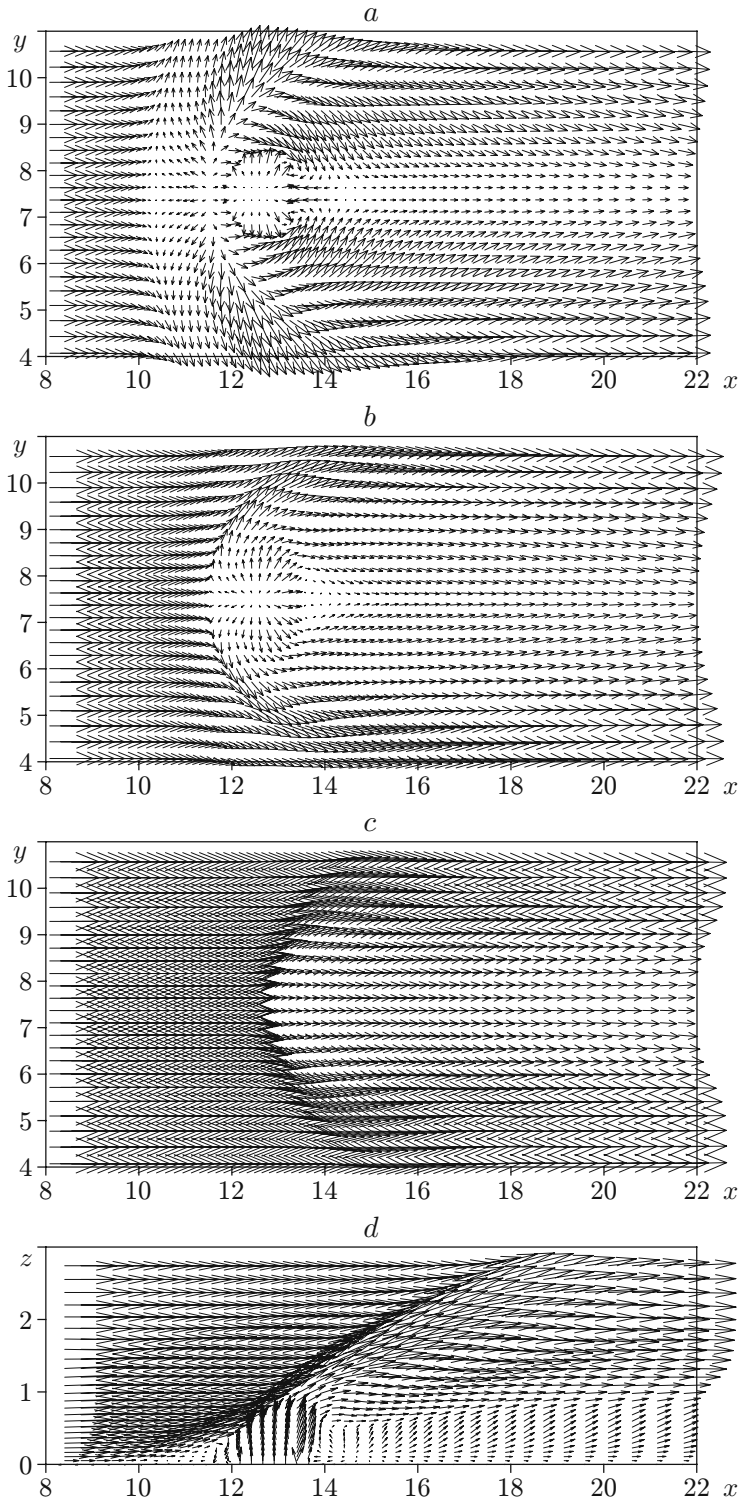

Fig. 3. Velocity field ($M_\infty = 4$, $M_0 = 1$, $n = 10$, $Pr = 0.9$, $Re = 10^4$, and $\gamma = 1.4$) in the plane x, y for $z = 0.15$ (a), 0.44 (b), and 1.01 (c) and in the symmetry plane x, z (d).

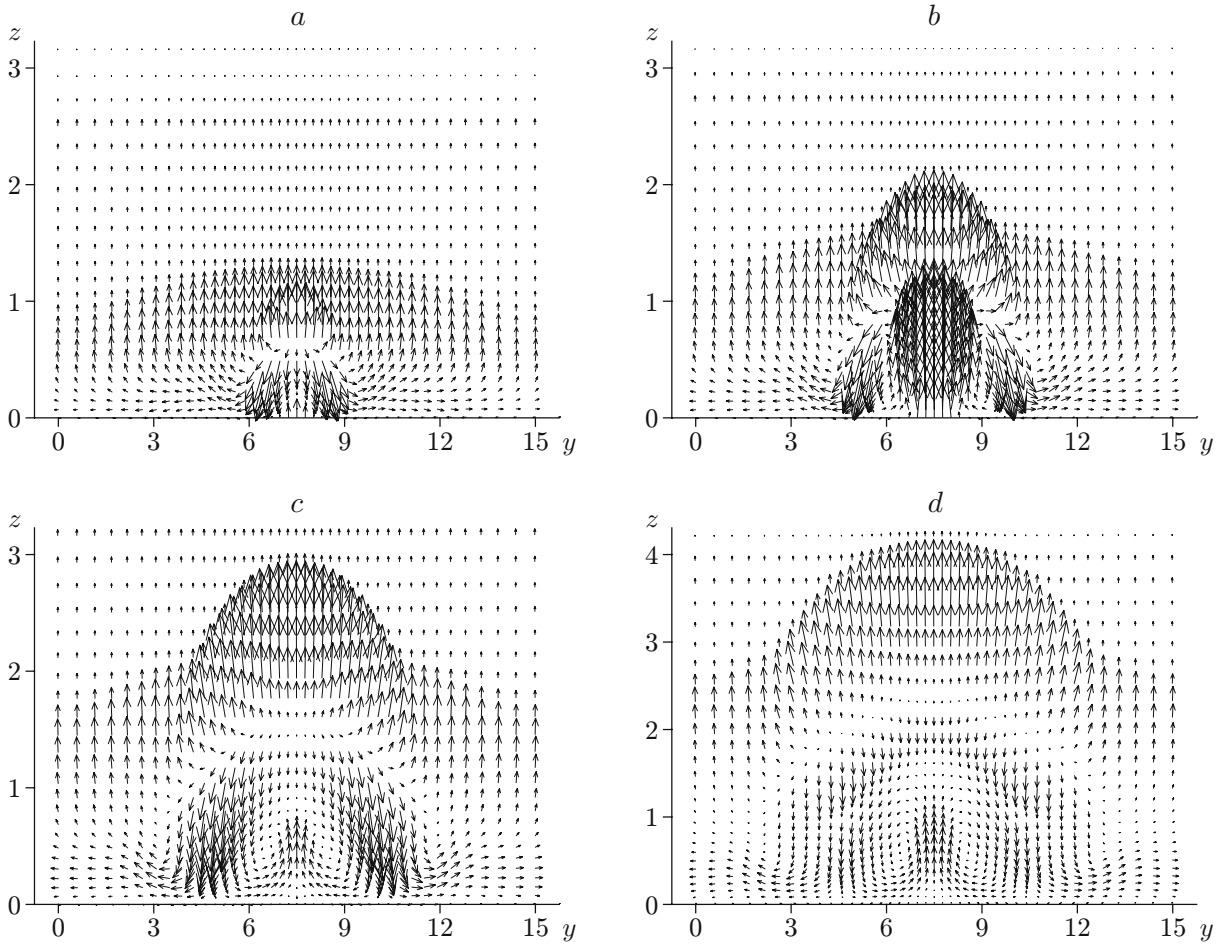

Fig. 4. Velocity vector field ($M_\infty = 4$, $M_0 = 1$, $n = 10$, Pr = 0.9, $Re = 10^4$, and $\gamma = 1.4$) in the plane y, z in different sections: $x = 11.70$ (a), 13.06 (b), 14.43 (c), and 21.72 (d).

this structure of the pressure field. In particular, it is seen in Fig. 2a that in the high-pressure zone in front of the jet, the isobars are nested ellipses. In addition, in Fig. 2a, one can see the boundary of the oblique shock (line 5 in Fig. 1). The lines of the terminal shock (line 7 in Fig. 1) are adjacent to the jet.

The resulting pressure distributions are consistent with the distributions of the local Mach number $M = \sqrt{u^2 + v^2 + w^2}/a$ (a is the local speed of sound) (see Figs. 2b, 2d, and 2f). In particular, one can clearly see the boundary of the injected jet and the supersonic zone near it, which arises as a result of acceleration of the flow which has enveloped the jet.

Nevertheless, although the flow which has enveloped the jet is accelerated behind the jet, a tail shock is not formed.

In studies of the jets issuing into supersonic flow, the question arises of the depth to which the jet penetrates into the flow. At present, it is known that the penetration depth does not depend uniquely on the ratio of the momentum of the jet to that of the oncoming flow [1–3]. The depth of penetration of the injected jet can be estimated from the velocity fields shown in Fig. 3. From Fig. 3a, it follows that the flow near the wall has clearly defined boundaries (shown in Fig. 1), whose position is consistent with experimental data [1].

In Fig. 3b, it is evident that the size of the separation zone in front of the jet decreases due to a decrease in the thickness of the subsonic boundary layer and closely approaches the injected jet; accordingly, the flow region around the jet narrows. Numerical experiments show that as the pressure ratio decreases to $n = 4$ in the section $z = 0.44$, the separation zone disappears.

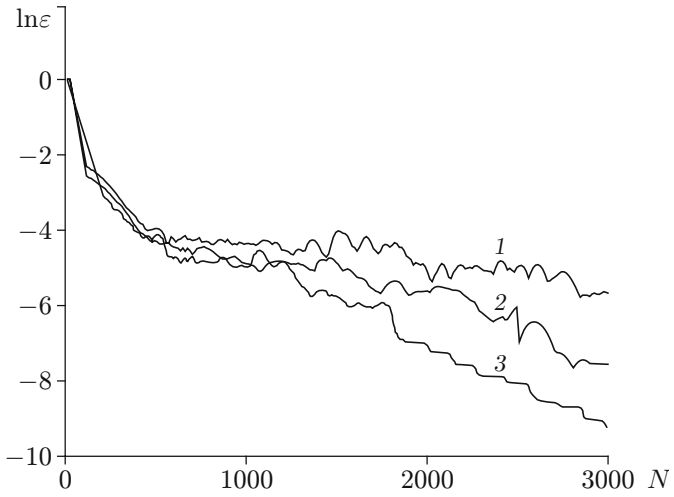

Fig. 5

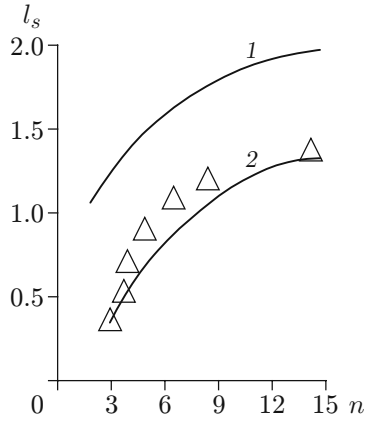

Fig. 6

Fig. 5. Dynamics of the dimensionless norm of the residual of the gas density for $M_\infty = 4$, $M_0 = 1$, $n = 10$, $Pr = 0.9$, $Re = 10^4$, $\gamma = 1.4$, and different grid sizes: $144 \times 66 \times 52$ (1), $181 \times 81 \times 66$ (2), and $201 \times 101 \times 81$ (3).

Fig. 6. Length of the separation zone l_s versus pressure ratio for $M_\infty = 3$, $M_0 = 1$, $Re = 1.87 \cdot 10^7$, $n = 15$, and $d = 1.4$ cm: curves 1 and 2 refer to the plane and three-dimensional problems; the points refer to the experimental data of [1].

In Figs. 3c and 3d, one can see that the separation zone in front of the jet is absent and the flow passes over the obstacle (jet). This indicates that in the section $z = 1.01$, the jet is in the flow. From the results of the calculations, it follows that in this case, the maximum depth of jet penetration is 0.91, whereas for $n = 4$, its value is 0.58.

Thus, the numerical experiments show that, as in the plane problem [10], the jet penetration depth and the size of the vortex zone in front of is depend greatly on the pressure ratio in the jet and flow.

The velocity field in the jet injection region given in Fig. 4 provides an understanding of the formation of lateral vortices in this zone. In the zone ahead of the jet, i.e., at a distance from the computational domain equal to $x = 11.7$ caliber (see Fig. 4a), there is a significant upward deflection of the flow and its spreading. From Fig. 4b ($x = 13.06$), it is evident that in the region of the injected jet, the flow is rapidly expanding. It follows from Fig. 4 that upon collision of the oncoming flow with the expanding jet, part of the flow turns to the nozzle. As a consequence, two symmetric vortices arise on both sides of the injected jet. The center of rotation of the vortices is located outside the expanding jet, and, hence, the vortices are formed in the layer of mixing of the jet and the flow. In addition, above the injected jet, the oncoming flow is deflected upward due to the presence of the bow shock wave.

The calculation results show that the behind the injected jet, the oncoming flow moves toward the plane of symmetry to form two systems of vortex wakes (see Fig. 4c and d). It is obvious that the vortices adjacent to the bottom wall are in the horizontal vortex wake behind the jet. In Fig. 4d, it is seen that at a sufficient distance downstream, these vortices almost disappear whereas the other vortex system is stable.

Figure 5 shows the dynamics of convergence of the numerical solution of the problem for the following grid sizes (N is the number of iterations): $144 \times 66 \times 52$, $181 \times 81 \times 66$, and $201 \times 101 \times 81$. The values of z_1^+ for these grids ($z_1^+ = z\,\mathrm{Re}\sqrt{c_f/2}$, where $c_f = 0.059(x\,\mathrm{Re})^{-0.2}$ [12]) are equal to 60, 50, and 38, respectively. In Fig. 5, it is seen that the minimum value of ε decreases significantly and the rate of convergence of the solution increases.

Figure 6 shows the results of the numerical experiment for the formulated problem ($M_\infty = 3$, $M_0 = 1$, diameter of the hole $d = 1.4$ cm, $Re = 1.87 \cdot 10^7$, the distance from the front sharpened edge of the plate on which there is the center of the jet, $x_0 = 14$ cm). These results were compared with the experimental data of [1]. Because in the experiment, the pressure ratio was in the range $1.2 \leqslant n \leqslant 130.0$ and in the calculations, the pressure ratio was $3 \leqslant n \leqslant 15$, the comparison was made only for the range $3 \leqslant n \leqslant 15$. From Fig. 6, it follows that the behavior of

the curve of $l_s(n)$ is the same in the two-dimensional and three-dimensional cases. However, in the two-dimensional case, the values of l_s are larger, due to the absence of spreading in the plane problem. The calculation results for the three-dimensional problem are in good agreement with the experimental data.

Conclusions. The problem of transverse injection of a round jet into supersonic flow was solved using Favre-averaged Navier–Stokes equations for a perfect gas. The dependence of the jet penetration depth on the pressure ratio was studied, and the mechanism of formation of a vortex wake behind the injected jet was determined. The numerically obtained velocity fields on the surface of the plate are in qualitative agreement with experimental data. Experimental dependences of the length of the separation zone on the pressure ratio were given.

REFERENCES

1. A. I. Glagolev, V. I. Zubkov, and Yu. A. Panov, "Supersonic flow over a gas jet obstacle on a plate," *Izv. Akad. Nauk SSSR, Mekh. Zhidk. Gaza*, No. 3, 97–102 (1967).
2. V. S. Avduevskii, K. I. Medvedev, and M. N. Polyanskii, "Interaction of supersonic flow with a transverse jet injected through a circular hole in a plate," *Izv. Akad. Nauk SSSR, Mekh. Zhidk. Gaza*, No. 5, 193–197 (1970).
3. A. I. Glagolev, A. I. Zubkov, and Yu. A. Panov, "Interaction of a gas jet flowing from a hole in a plate with supersonic flow," *Izv. Akad. Nauk SSSR, Mekh. Zhidk. Gaza*, No. 2, 99–102 (1968).
4. J. R. Drummond and E. H. Weidner, "Numerical study of a ramjet flow field," *AIAA J.*, **20**, No. 9, 1182–1187 (1982).
5. J. S. Shuen and S. Yoon, "Numerical study of chemically reacting flows using a lower-upper symmetric overrelaxation scheme," *AIAA J.*, **27**, No. 12, 1752–1760 (1989).
6. R. Ramakrishnan and D. J. Singh, "Modeling scramjet combustor flowfields with a grid adaptation scheme," *AIAA J.*, **32**, No. 5, 930–935 (1994).
7. F. Grasso and V. Magi, "Simulation of transverse gas injection in turbulent supersonic air flows," *AIAA J.*, **33**, No. 1, 56–62 (1995).
8. C. F. Chenault and P. S. Beran, "Numerical investigation of supersonic injection using a Reynolds stress turbulence model," *AIAA J.*, **37**, No. 10, 1257–1269 (1999).
9. Sun De-chuan, Hu Chun-bo, and Cai Ti-min, "Computation of supersonic turbulent flowfield with transfer injection," *Appl. Math. Mech.*, **23**, No. 1, 107–114 (2002).
10. A. O. Beketaeva and A. Zh. Naimanova, "Numerical simulation of a supersonic flow with transverse injection of jets," *J. Appl. Nech. Tech. Phys.*, **45**, No. 3, 367–374 (2004).
11. C. A. Fletcher, *Computational Techniques for Fluid Dynamics*, Springer (1988).
12. G. Schlichting, *Boundary-Layer Theory*, McGraw-Hill, New York (1968).
13. T. J. Poinsot and S. K. Lele, "Boundary conditions for direct simulation of compressible viscous flows," *J. Comput. Phys.*, No. 101, 104–129 (1992).
14. R. M. Beam and R. F. Warming, "An implicit factored scheme for the compressible Navier–Stokes equations," *AIAA J.*, **16**, No. 4, 393–402 (1978).
15. D. Anderson, J. Tannehil, and R. Pletcher, *Computational Fluid Mechanics and Heat Transfer*, Hemisphere, New York (1984).